Journal of Catalysis 287 (2012) 37–43

Contents lists available at SciVerse ScienceDirect

Journal of Catalysis

journal homepage: www.elsevier.com/locate/jcat

Correlation of Pt–Re surface properties with reaction pathways for the aqueous-phase reforming of glycerol

Liang Zhang [a], Ayman M. Karim [a], Mark H. Engelhard [a], Zhehao Wei [b], David L. King [a,*], Yong Wang [a,b,*]

[a] Institute for Integrated Catalysis, Pacific Northwest National Laboratory, 902 Battelle Blvd., Richland, WA 99352, United States
[b] The Gene and Linda Voiland School of Chemical Engineering and Bioengineering, Washington State University, Pullman, WA 99164, United States

ARTICLE INFO

Article history:
Received 4 August 2011
Revised 21 November 2011
Accepted 22 November 2011
Available online 17 January 2012

Keywords:
Aqueous-phase reforming
Surface acidity
Pt–Re/C catalyst
Pt–Re interactions
C–C bond cleavage
C–O bond cleavage
Re oxidation
Ammonia TPD

ABSTRACT

The surface properties of Pt–Re catalytic nanoparticles supported on carbon following exposure to a hydrogen reducing environment and subsequent hydrothermal conditions have been studied using *in situ* X-ray photoelectron spectroscopy (XPS) and ammonia temperature-programmed desorption (TPD). These properties have been correlated with the catalyst selectivity for the aqueous-phase reforming of glycerol. We show that Pt in reduced Pt–Re/C becomes electron deficient, and a fraction of the Re becomes oxidized when the catalyst is subsequently exposed to hydrothermal reaction conditions. Oxidation of Pt–Re generates surface acidity, which drastically affects the reaction pathways. The acid site concentration, but not acid site strength, increases with Re loading. This acidity increase with Re addition favors C–O over C–C cleavage, which results in higher selectivity to liquid products and alkanes at the expense of hydrogen selectivity. We propose a model for the Pt–Re active site and the origin of acidity enhanced by the addition of Re.

1. Introduction

Production of hydrogen through the aqueous-phase reforming (APR) of biomass-derived oxygenated hydrocarbons (sugars, sugar alcohols, polyols, etc.) is considered a promising catalytic process and has attracted academic and industrial interest. Important advantages of the APR process include its low energy consumption, since APR proceeds at lower temperatures than conventional steam reforming, and its compatibility with the use of wet feedstocks, avoiding any predrying step [1]. A variety of catalyst formulations have been proposed and tested by several groups for the APR process [2–10]. Precious metals such as Pt are preferred catalysts due to their high selectivity in breaking C–C bonds [11]. The catalyst activity in the APR reaction can be enhanced by doping precious metals with other transition metals [9,10,12,13]. For example, our recent work has shown that addition of Re to Pt/C substantially increases conversion of glycerol in the aqueous phase by at least one order of magnitude [14]. However, the role of Re and nature of active sites are still not fully understood.

APR of biomass-derived liquids normally involves reforming followed by water gas shift (WGS) of the CO produced. Literature reports indicate that Re addition to Pt-based catalysts supported on metal oxides increases activity for the WGS reaction. Two theories have been provided for the observed enhanced activity. The first is Pt–Re alloy formation [15–17], and the second involves the role of ReO_x species [18,19]. One effect of Pt–Re alloy formation that has been in debate is the strength of CO adsorption, with the idea that too strong CO chemisorption increases CO site coverage and decreases the availability of operating WGS sites. Therefore, weaker adsorption strength could result in higher activity. There have been both reports of stronger [15] and weaker CO adsorption [13,20] compared to pure Pt. These contradictory reports could be due to particle size effects. Ruettinger et al. reported that CO adsorption is weaker on small Pt–Re particles and stronger on the larger Pt–Re particles [16]. An alternative theory has been proposed wherein ReO_x species are present and provide a redox route for the WGS reaction, in which ReO_x is reduced by CO, generating CO_2, and re-oxidized by H_2O, forming H_2 [18].

Analogous to the examination of Re promotion of Pt catalysts for the WGS reaction, Kunkes and coworkers studied the structure of reduced Pt–Re supported on carbon for the glycerol steam reforming reaction. They proposed formation of a Pt–Re alloy phase or a surface having close contact between the Pt and Re phases and measured a lower CO binding energy compared with Pt alone, thus allowing more sites to be available for reforming [13,21]. However, the lower CO binding energy was measured on

* Corresponding authors. Address: Institute for Integrated Catalysis, Pacific Northwest National Laboratory, 902 Battelle Blvd., Richland, WA 99352, United States.
E-mail addresses: david.king@pnl.gov (D.L. King), yongwang@pnl.gov (Y. Wang).

0021-9517/$ - see front matter © 2011 Elsevier Inc. All rights reserved.
doi:10.1016/j.jcat.2011.11.015

partially oxidized Pt–Re using 2% O_2 at 100 °C followed by reduction at 70 °C prior to the CO-TPD [13].

In this work, we provide characterization of Pt–Re under conditions similar to that encountered during APR in an effort to obtain an improved understanding of the role of Re. We specifically focus on investigation of the structure of Pt–Re/C catalysts under environments that simulate APR reaction conditions and on the correlation of catalyst structure to product distribution. XPS results suggest that hydrogen reduction results in the formation of bimetallic Pt–Re with Pt slightly positively charged. Under an environment similar to APR reaction conditions, XPS shows that the Re in the bimetallic is substantially oxidized. NH_3 adsorption further reveals that the Pt–Re interaction following exposure to water vapor results in acidity generation that affects the reaction pathways. We show that the prevalence of the dehydration pathways, relative to decarbonylation (C–C bond cleavage), is related to the strength and number of surface acid sites. Surface acidity on bimetallic catalysts such as Pt–Re and Rh-Re has been recently reported [22,23].

2. Materials and methods

The catalysts were prepared by sequential incipient wetness impregnation of tetra-amine platinum nitrate and perrhenic acid (Alfa Aesar). A high surface area activated carbon support (Engelhard, SSA 540 m^2/g, pore volume 0.42 ml/g) was selected for this work. Specifically, for synthesis of the 3 wt%Pt/C catalyst, 20 g of the dried carbon support was impregnated with a solution prepared by dissolving 1.24 g of $Pt(NH_3)_4(NO_3)_2$ into 8.4 g of DI water in a 30-ml glass vial, with shaking for at least 2 h prior to use. The impregnated sample was dried at 110 °C in air for 2 h and then calcined at 260 °C in air for 2 h with a ramp rate of 5 °C/min. Pt/C catalysts with different loadings were prepared analogously. For preparation of Pt–*X*wt%Re/C catalysts (*X* ranges from 1 to 4.5), the perrhenic acid solution was impregnated on the prepared Pt/C in a subsequent step, with analogous pretreatment.

XPS measurements were made using a Physical Electronics Quantum 2000 Scanning ESCA Microprobe. This system uses a focused monochromatic Al Kα X-ray (1486.7 eV) source and a spherical section analyzer. The X-ray beam (100 μm diameter) is incident normal to the sample, rastering over a 1.3 mm by 0.2 mm rectangular area. The photoelectron detector was at 45° off-normal using an analyzer angular acceptance width of 20° × 20°. High-energy-resolution spectra were collected using a pass energy of 46.95 eV. The energy scale of the analyzer was calibrated using sputter-cleaned Cu and Ag foils. For the Ag $3d_{5/2}$ line, these conditions produced FWHM of better than 0.98 eV. The binding energy (BE) scale is calibrated using the Cu $2p_{3/2}$ feature at 932.62 ± 0.05 eV and Au 4f at 83.96 ± 0.05 eV from known standards. In an attempt to neutralize any charge buildup during the analysis, the samples were exposed to low-energy electrons (about 1 eV) and low-energy Ar^+ ions. However, the surface charging could not be completely eliminated, and therefore, we used C 1s binding energy at 284.5 eV as a reference to correct for the charging. The instrument is equipped with a side chamber that allows *in situ* sample treatment with various gases with programmed temperature profiles and the transfer of the samples to the XPS chamber without exposure to air. A 7-sample Mo holder is used to transfer the samples between the XPS analysis chamber and the side chamber using a magnetic transfer arm. Samples were sequentially treated with 100 sccm H_2 flow at 80 °C and 280 °C for 1 h and exposed to 100 Torr water vapor at 225 °C for 1 h. After each treatment, the samples were transferred to the XPS chamber for spectra collection.

NH_3 temperature-programmed desorption was carried out using an Autochem II pulse chemisorption (Micromeritics) unit and mass spectrometer (MS) analyzer (Pfeiffer); 100 mg of catalyst was used for each TPD experiment. The catalyst was reduced in 50 sccm H_2 at 280 °C for 1 h, and then the sample was purged with 50 sccm N_2 for 30 min and the temperature cooled to 225 °C. N_2 flow through a water bubbler at room temperature was used to treat the catalyst with water vapor at 225 °C through several pulses. The water partial pressure in each pulse was about 20 Torr. The H_2O pulsing was repeated until no more H_2O uptake was detected using the MS.

APR reactions were carried out in a single-channel microreactor with active heat exchange to maintain near isothermal conditions within the catalyst bed as previously described [14,24]. The microchannel reactor body was made from SS316 and was enclosed by an oil-heating jacket with the oil being circulated using a Julabo oil pump. The reaction temperature was controlled within ±1 °C. The total effective volume of the reactor channel was about 0.45 ml (0.635 mm × 12.7 mm × 55 mm). A charge of 200 mg catalyst (60–100 mesh) was packed into the narrow slot of the microchannel reactor, and a stainless steel screen (−325 mesh) and a stainless steel foam disk were placed on each side of the reactor to maintain the catalyst particles in place during experiments.

Prior to the reaction test, the catalyst was reduced at 280 °C for 2 h in pure H_2 (20 sccm) at atmospheric pressure and cooled down to room temperature. After purging the system with N_2 for 30 min, the backpressure regulator was set at the reaction pressure (425 psig), the aqueous feed solution comprising 10% glycerol (by weight) was introduced using a HPLC digital pump (Series III) at the desired feed rate, and heating of the catalyst bed was initiated. When the reactor reached the reaction temperature of 225 °C, N_2 flow was set at 20 sccm (N_2 served as an internal analytical standard). The system was allowed to stabilize for about 2 h prior to analysis of the reaction products. Gas product analysis was carried out using a micro gas chromatograph (Agilent Micro GC 3000C) equipped with four channels, one molecular sieve 5A column, one Plot Q column, and two OV-1 columns. The liquid products were collected and analyzed with a Waters high-performance liquid chromatograph (HPLC). A Bio-Rad Aminex HPX-87H ion exclusion column (300 mm × 7.8 mm) was used for analyte separation. A 0.005 M H_2SO_4 aqueous solution was used as eluent for this analysis at a flow rate of 0.55 ml/min. Carbon balance was typically greater than 95%.

3. Results and discussion

3.1. APR of glycerol on Pt/C and Pt–Re/C

As reported previously [13], Pt/C and Pt–Re/C behave differently in aqueous-phase reforming of glycerol. Addition of Re to Pt significantly enhances conversion of glycerol as evidenced by more than 10 times increase in TOF of glycerol (based on CO chemisorption), as shown in Fig. 1. As also can be seen in Fig. 1, addition of Re to Pt changes the distribution of products. Specifically, the presence of Re increases the selectivity toward C_2^+ alkanes and alcohols (ethanol and propanol), along with the production of carboxylic acids, at the expense of hydrogen, carbon dioxide, and diols (ethylene glycol (EG) and propylene glycol (PG)) selectivity. As a comparison, APR experiments were also conducted on Re/C and a physical mixture of Pt/C plus Re/C, Table 1. Re/C showed a much lower activity than Pt/C, while the physical mixture of Pt/C and Re/C exhibited a similar activity to Pt/C, indicating no synergistic effect by Re without close contact between Pt and Re. In order to understand the role of Re in changing the product distribution, we studied the surface properties of Pt–Re, in particular under hydrothermal conditions.

3.2. Oxidation state change for Pt–Re/C catalysts

To understand Pt–Re interaction on the Pt–Re/C catalyst during the APR reaction, we examined the electronic structure of Pt and Re

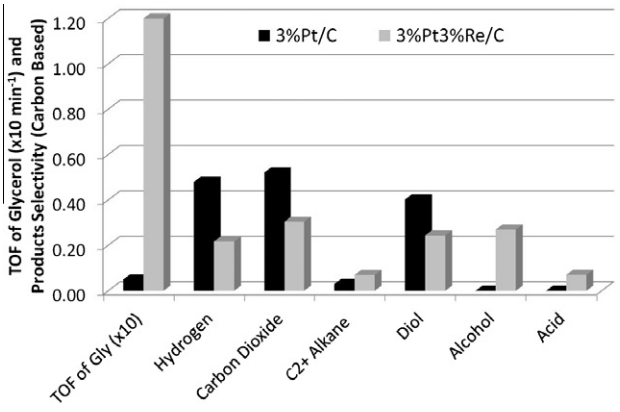

Fig. 1. TOF of glycerol (min^{-1}, based on CO chemisorption) and selectivity toward products (based on carbon) for aqueous-phase reforming of 10% glycerol over 3%Pt/C and 3%Pt–3%Re/C at 225 °C and 420 psig. The selectivity to H_2 is defined as the hydrogen produced relative to the maximum that could be produced if all the reacted glycerol were converted to H_2 and CO_2. Space velocity (WHSV: gram glycerol/gram catalyst/hr) was held at 1.5 for Pt/C and 15 for Pt–Re/C to achieve a similar conversion level (30%).

in Pt–Re/C catalysts using XPS after hydrogen pretreatment followed by exposure to water vapor. With the *in situ* treatment capability of the XPS instrument, we were able to track the changes in the oxidation states of Pt and Re in Pt–Re/C catalysts after designated treatments without exposure to air. All spectra shown were calibrated to C 1s at 284.5 eV. Fig. 2 shows Pt $4f_{7/2}$ and Re $4f_{7/2}$ spectra of a series of catalysts after reduction. The Pt $4f_{7/2}$ binding energy of both calcined 3%Pt/C and 3%Pt–X%Re/C was measured at 72.85 eV (not shown), which was assigned to PtO [25]. When 3%Pt/C was reduced at 280 °C, the Pt $4f_{7/2}$ binding energy shifted to 71.52 eV. This peak could be assigned to zero-valent Pt, although it is 0.7 eV higher than bulk Pt metal, possibly due to metal–support interaction or a cluster size effect [26,27]. The addition of Re results in a clear shift of Pt^0 binding energy, and the shift increases with the amount of Re in the catalyst. After deconvolution of the Pt 4f peaks, the Pt $4f_{7/2}$ binding energy for the series of catalysts was quantified and plotted against the fraction of Re in Pt–Re as shown in Fig. 3. It can be seen that the Pt $4f_{7/2}$ binding energy shift is proportional to the amount of Re in the catalyst. Some studies have proposed that Pt and Re form an alloy upon reduction [13,28,29]. The increase in electron deficiency of Pt observed in this work may be a result of the formation of a Pt–Re alloy. It should be emphasized that Re was impregnated on a presynthesized and calcined Pt/C, and Pt particle size for catalysts with various Pt/Re ratios is the same prior to Re addition. The size of Pt-associated particles would be expected to increase upon addition of Re due to the formation of the Pt–Re alloy. Therefore, the increase in binding energy shift is mainly due to the Pt–Re interaction and not due to (a decrease in) Pt particle size. Additionally, EDS analysis has been performed on individual particles in our Pt–Re/C catalysts (EDS results on reduced catalyst are shown in the Supplementary information, Figs. 2 and 3), and the Pt/Re ratio was uniform within each particle, consistent with the formation of a Pt–Re alloy. It should be noted that for a Pt–Re alloy, one would expect the trend in Re $4f_{7/2}$ binding energy to be opposite to that of Pt $4f_{7/2}$. However, the Re $4f_{7/2}$ binding energy was higher for the Pt–Re/C catalysts compared to the Re/C catalyst and was in the range of 40.8 eV to 41 eV, close to $4f_{7/2}$ of Re^0 as reported by Shpiro et al. [30]. It appears that Re addition results in both Pt and Re becoming more electron deficient, possibly due to carbon–metal interactions, wherein the extent of Pt electron deficiency is proportional to the Re amount in the catalyst.

In this study, the feed was 10 wt% glycerol in water. The molar ratio of water to glycerol was about 50:1. Therefore, in the condensed phase at elevated temperature (200–250 °C for APR reaction), the role of water on the Pt–Re interaction must be considered. To simulate APR conditions, a stream of water vapor was fed into the XPS side chamber where Pt–Re/C catalysts were previously reduced. A dramatic change in oxidation state was

Table 1
Comparative conversion and selectivity values for the APR of glycerol over Pt/C, Pt–Re/C, and Re/C catalysts. Reaction conditions: 225 °C, 420 psig, WHSV = 6 h^{-1}.

	3%Pt/C unreduced	3%Pt/C reduced	3%Pt–3%Re/C unreduced	3%Pt–3%Re/C reduced	Physical mix reduced	3%Re/C reduced
Conversion	8.2%	7.4%	6.7%	68.2%	10.1%	2.6%
C–O/C–C	0.6	0.6	0.5	1.1	1.0	33.8
H_2/CO_2	2.3	2.3	2.3	2.0	1.8	

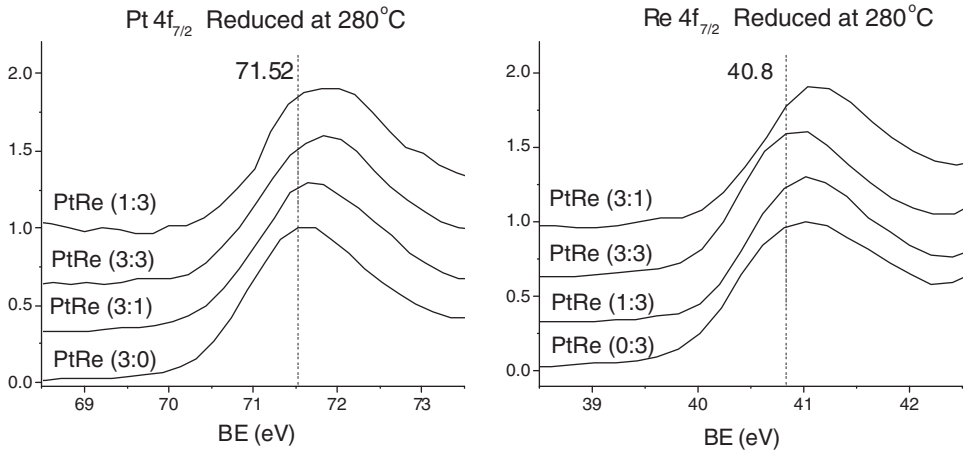

Fig. 2. XPS spectra of Pt/C, Re/C, and Pt–Re/C catalysts with different ratios (based on weight percentage of metal). All the catalysts were reduced at 280 °C. Dashed lines label the binding energy for Pt^0 $4f_{7/2}$ (71.52 eV) in 3%Pt/C, and for Re^0 $4f_{7/2}$ (40.8 eV) in 3%Re/C, obtained by peak fitting.

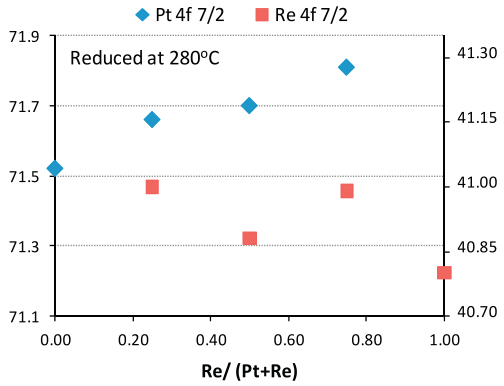

Fig. 3. Binding energies of Pt $4f_{7/2}$ and Re $4f_{7/2}$ for Pt/C, Re/C, and Pt–Re/C catalysts reduced at 280 °C.

subsequently found for both Pt and Re, as shown in Fig. 4. Pt was partially oxidized by water in both Pt/C and Pt–Re/C (Fig. 4a and b), indicating that Pt–O or Pt–OH might participate in glycerol conversion. The left panel in Fig. 5 shows a shift in Pt $4f_{7/2}$ binding energy for Pt–Re/C catalysts with varying Pt/Re ratios. The Pt $4f_{7/2}$ binding energy of water vapor–treated catalysts follows a similar trend as for the reduced catalysts, and the shift in Pt $4f_{7/2}$ binding energy increases with the amount of Re. Water treatment also results in oxidation of Re in the Pt–Re catalysts. As shown in Figs. 4c and 5 (right panel), Re is oxidized to a mixture of oxidation states, which may include 2+, 4+, 6+, and 7+. The oxophilicity of Re has been reported in the literature. A study by Fusy et al. showed that water readily dissociated on the surface of Re at room temperature with generation of atomic O and OH radicals [31]. Surprisingly, after exposure to water vapor, Re/C is less oxidized than Re in Pt–Re/C catalysts (right panel of Fig. 5). This suggests that addition of Pt facilitates the oxidation of Re.

3.3. Surface acidity of oxidized Pt–Re/C

The oxidation of Pt and Re by steam has important implications for the structure of Pt–Re under APR conditions. One possibility is the generation of surface acidity. In order to measure the number of surface acid sites and relative acid strength, we carried out NH_3 adsorption measurements on the Pt–Re/C catalysts with different Pt/Re ratios. Prior to the base titration, the catalysts were treated under conditions similar to the *in situ* XPS experiments. The left panel in Fig. 6 shows the NH_3 adsorption capacity for catalysts reduced at 280 °C and exposed to 20 Torr water vapor (balance Ar at atmospheric pressure) at 225 °C. To establish a baseline, blank carbon was also treated in the same way as other catalysts and saturated with ammonia; negligible ammonia desorption was detected, as shown. It can be seen that the ammonia desorption peak from Pt/C centers at 136 °C while ammonia desorption on Pt–Re/C shows one peak centered at 188 °C with a shoulder at 108 °C for all catalysts. Based on the location of the major desorption peaks, the acid strength of Pt/C is less than that of Pt–Re/C. The type or distribution of acid sites is difficult to determine, as characterization by FTIR of adsorbed probe molecules such as CO, NH_3, or pyridine is not applicable to carbon-supported catalysts. However, separate infrared studies on silica-supported Pt–Re suggest that Brønsted acid sites form after the catalyst is first reduced followed by exposure to steam (see Supplementary information, Fig. 4 and related discussion). The number of acid sites was measured by integrating the area under the TPD curves, and the results are shown in the right panel of Fig. 6. The ammonia capacity increased linearly with the loading amount of Re in Pt–Re/C catalysts. The ratio of acid to metal sites was between 0.37 and 0.44 for the Pt–Re/C catalysts, while it was 0.18 for the 3%Pt/C catalyst. The XPS results on Re/C after reduction and exposure to steam had shown less oxidation compared to Re in Pt–Re/C. Analogously, the Re/C showed lower NH_3 capacity than Pt–Re/C catalysts as shown in Fig. 6. The XPS results, low ammonia capacity on Re/C, and the linear relation between the Re loading on Pt/C and the number of acid sites all imply that the acid sites mainly evolved from Pt–Re interaction, which could be ascribed to increasing number of surface-oxidized Pt–Re. The introduction of surface acidity by Re was reported earlier [22], and the addition of KOH was shown to neutralize the acid sites [14,22]. More recently, Chia et al. showed that the acidity introduced by ReO_x was responsible for the enhanced C–O hydrogenolysis on Re–Rh/C catalysts [23]. However, we believe that the acidity is introduced through a Pt–O–Re structure rather than a ReO_x species as will be discussed below. One of the possible structures of oxidized Pt–Re in the presence of water is shown in Fig. 7. Pt–Re may be oxidized by dissociated water with OH attached to Re. Because of the oxophilic nature of Re, Re–OH may function as a Brønsted acid site, while nearby Pt could provide a Lewis acid site due to its electron deficiency. Another evidence for oxidized Pt–Re as acid site and active site resides in solubility of ReO_x. It is well known that Re VII readily dissolves in water. ICP analysis of the

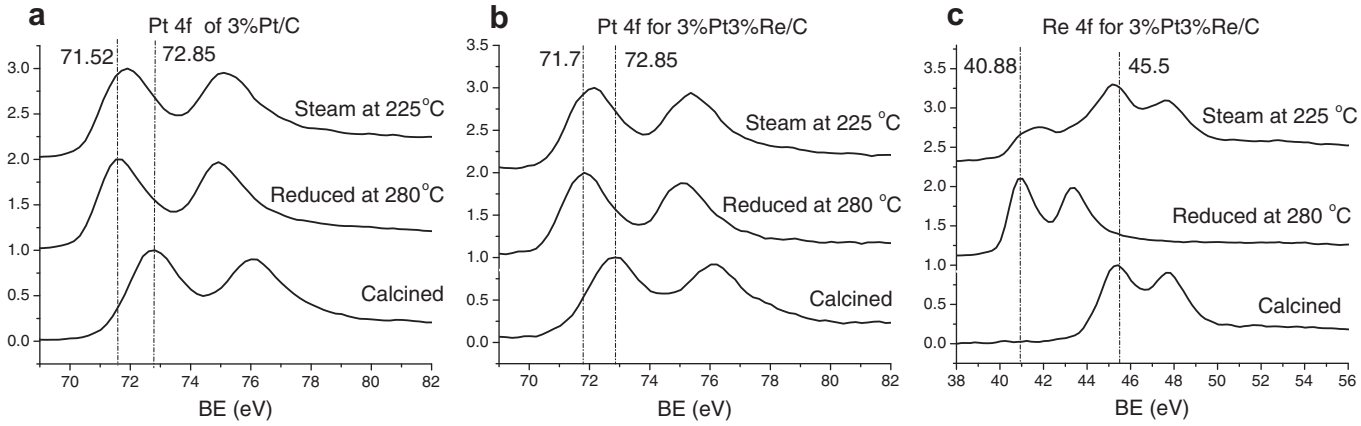

Fig. 4. XPS spectra of 3%Pt/C and 3%Pt–3%Re/C catalysts acquired after sequential treatments: calcination at 260 °C, reduction at 280 °C, and exposure to steam at 225 °C. The doublets in most of the spectra correspond to the $4f_{7/2}$ (lower energy) and $4f_{5/2}$ (higher energy) peaks. The left dashed line in the figures corresponds to the $4f_{7/2}$ values for Pt^0 in 3%Pt/C and 3%Pt-3%Re/C in 4(a) and 4(b), respectively, and the $4f_{7/2}$ value for Re^0 in 3%Pt-3%Re/C in 4(c), all obtained by peak fitting. The right dashed lines correspond to Pt^2 in bulk PtO and Re^{7+} in bulk Re_2O_7. A shift in the binding energy is clearly seen following addition of steam at 225 °C. A smaller but similar shift was seen with lower steam partial pressure.

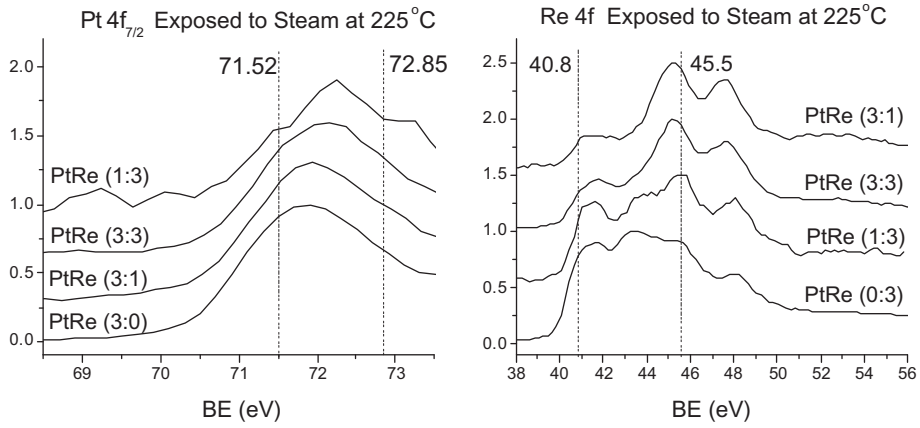

Fig. 5. XPS spectra of Pt/C, Re/C, and Pt–Re/C catalysts with different ratios (based on weight percentage of metal). All the catalysts were reduced at 280 °C and exposed to water vapor at 225 °C. Left dashed lines correspond to the binding energies for Pt^0 $4f_{7/2}$ in 3%Pt/C and Re^0 $4f_{7/2}$ in 3%Re/C reduced at 280 °C, obtained by peak fitting. The right dashed lines represent values for Pt^{2+} in bulk PtO and Re^{7+} in bulk Re_2O_7.

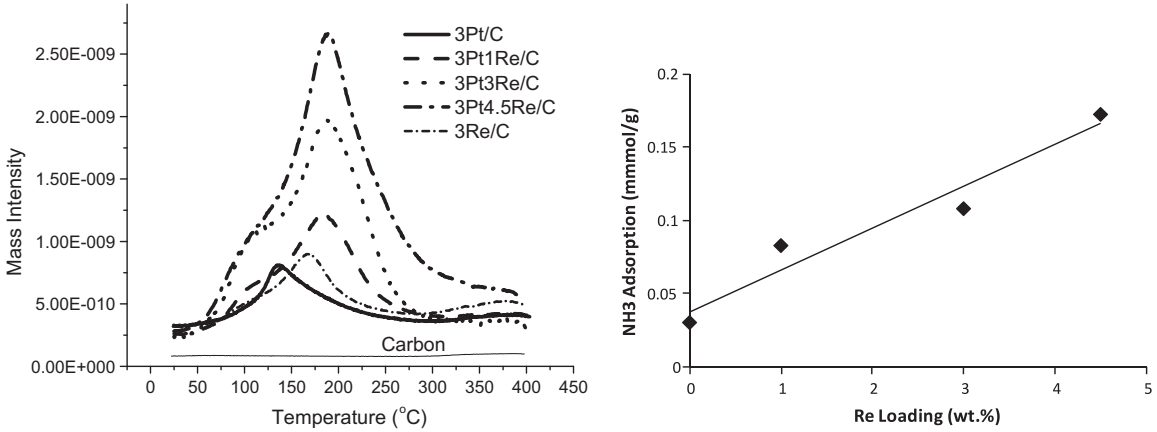

Fig. 6. Adsorption of NH_3 over Pt/C and Pt–Re/C catalysts with varying Pt/Re ratio along with Re/C: NH_3 TPD on the left panel and amount of adsorbed NH_3 as function of Re loading in the right panel. The NH_3 absorption on 3%Re/C is 0.03 mmol/g (not shown in the right panel), similar to 3%Pt/C. All the catalysts were reduced at 280 °C and saturated with water vapor at 225 °C prior to NH_3 adsorption.

spent 3%Pt–3%Re/C showed loss of about 50% of the Re; however, the catalyst activity and selectivity were only slightly changed over 100 h (as shown in Fig. 5 in Supplemental materials). The number of acid sites will be correlated with the catalyst activity and product distribution below.

3.4. Effect of the surface acidity of Pt–Re/C on the reaction pathways

Several papers have reported the selectivity of gas products and liquid products from APR of glycerol [13,32–34]. The complexity of products makes the analysis of reaction pathways based on individual products very difficult. We have previously proposed two major competing reaction pathways over the Pt–Re surface [14]: C–C cleavage through decarbonylation and C–O cleavage through dehydration followed by hydrogenation (since we do not see any unsaturated products, a hydrogenation step must also occur). Following this concept, a schematic network of reaction pathways is depicted in Fig. 8. To simplify the analysis and provide greater insight into the effect of Re on the reaction pathway, we define a new parameter of competition ratio to characterize the overall reaction results. The competition ratio is defined as the ratio of dehydration pathway events to decarbonylation pathway events and is calculated using the following equation, where the number of C–O bonds cleaved is divided by the number of C–C bonds cleaved:

$$\frac{\text{Dehydration}}{\text{Decarbonylation}} = \frac{\sum_i \text{moles of dehydrated product}_i \times \text{dehydration steps to reach product}_i}{\text{moles of } CO_2}$$

The dehydrated products include those derived directly or indirectly from one or more dehydration steps, while the decarbonylation pathway leads to the formation of CO_2 via water gas shift of

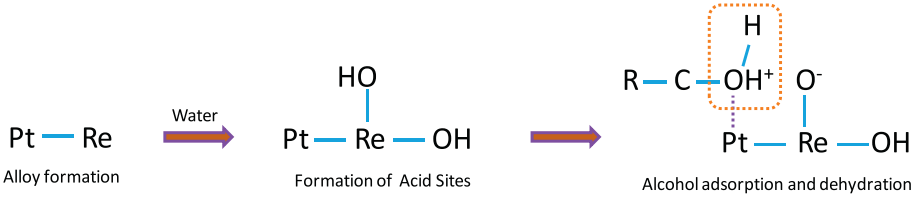

Fig. 7. One possible structure of oxidized Pt–Re in the presence of water. Upon exposure to water, Pt–Re dissociates water with hydroxyl groups attached to Re. Because of the oxophilic property of Re, OH tends to deprotonate. The dissociated proton may protonate adsorbed ROH to facilitate the dehydration reaction.

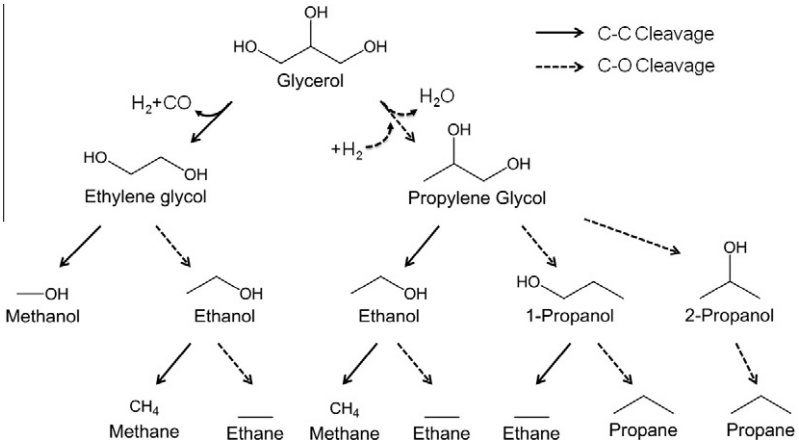

Fig. 8. Major reaction pathways for aqueous-phase reforming of glycerol.

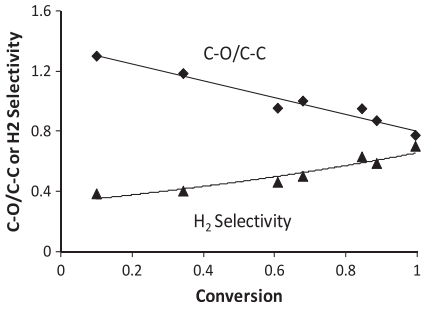

Fig. 9. Competition ratio (C–O/C–C) and H_2 selectivity as function of conversion on 3%Pt–3%Re/C.

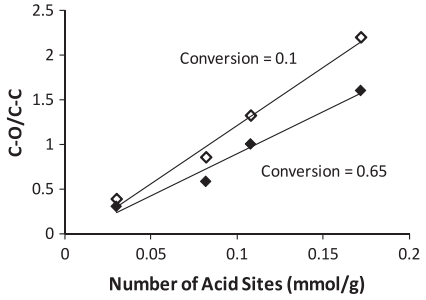

Fig. 10. Relation between C–O/C–C and number of acid sites on Pt/C and Pt–Re/C catalysts with different Pt/Re ratios.

CO. Ethylene glycol, methanol, and CO are pure decarbonylation products, whereas many products can be seen to be the result of a combination of dehydration and decarbonylation. For example, methane is considered a product derived from ethanol, and its formation includes one dehydration step (either dehydration of glycerol flowed by decarbonylation or dehydration of ethylene glycol) along with two decarbonylation steps (producing of two moles of CO_2).

Fig. 9 shows the competition ratio (C–O/C–C) and H_2 selectivity as a function of conversion for the 3%Pt–3%Re/C catalyst. The conversion was varied by changing the space velocity of the feed. Clearly, the competition ratio decreases with increasing conversion, and since the dehydration pathway is followed by hydrogenation, thereby consuming hydrogen, the H_2 selectivity also increases with increasing conversion. This trend could be due to a pool of intermediates formed at higher conversion, which are more difficult to dehydrate. For example, more diols and monohydric alcohols were found at higher conversion, and the dehydration of alcohols and diols was found to be less favored compared to dehydration of glycerol [14], leading to increased decarbonylation selectivity at higher conversion. Also, in other experiments (not shown), the dehydration selectivity (at similar conversion) during APR followed the order ethanol < ethylene glycol < glycerol. We found similar trends with the other Pt/C and Pt–Re/C catalysts and extrapolated the data in order to compare the competition ratio for the different catalysts at the same conversion. The results are presented in Fig. 10, and it is clear that the dehydration/decarbonylation ratio is proportional to the number of acid sites. The reaction medium is just mildly acidic (pH = 5–6), raising the possibility that media pH could have an effect on the dehydration pathways. However, in a separate experiment (not shown), addition of nitric acid showed no effect on Pt–Re/C catalyst activity or product selectivity despite the low pH of 2 during the reaction. Fig. 10 shows a linear relation between C–O/C–C cleavage reactions and number of surface acid sites, over a glycerol conversion range from 0.1 to 0.65. Therefore, it can be predicted that addition of base to the feed should neutralize the surface acid sites and depress the dehydration/hydrogenation pathways, increasing hydrogen productivity. This was confirmed by our previous work of glycerol reforming in the presence of KOH [14].

The question can be raised that the acidity of the system may be provided by Re/C particles in which the Re is not associated with Pt. We believe that the comparative data provided in Table 1, coupled with the NH_3 TPD results provided in Fig. 6, argue against this. The activity and total acidity provided by 3%Re/C are too low to contribute significantly to the overall results, and it appears that the Re associated with Pt generates more significant acidity in this system. Moreover, we measured by ICP the Pt and Re content of 3%Pt–3%Re/C after 1 week of tests and found that the Re content decreased by nearly 50%, whereas the Pt content was virtually unchanged. The corresponding catalyst activity decreased by about 10%, and the selectivity was nearly unchanged over this time (see Fig. 5, Supplemental information). Since Re^{7+} (Re_2O_7) is soluble in water, the effect of Re in contributing to C–O bond cleavage must come from its association with Pt, wherein it is stabilized relative to dissolution.

4. Conclusions

We have investigated the structure of Pt–Re/C catalysts with varying Re loadings following reduction and exposure to a simulated hydrothermal environment. When exposed to steam at elevated temperature, the Pt–Re catalyst undergoes oxidization. Our

results suggest that the active site during the APR reaction is not the Pt–Re alloy but is more likely to be based on oxidized Pt–Re. The Pt–Re interaction under hydrothermal conditions results in local surface acidity. The number of acid sites is proportional to the amount of Re in the Pt–Re catalysts. The surface acidity facilitates the dehydration pathway, with the ratio of dehydration to decarbonylation increasing linearly with number of surface acid sites. Our results show the importance of surface acidity in controlling the reaction pathways during aqueous-phase reforming.

Acknowledgements

The authors acknowledge financial support from the US Department of Energy, Office of Energy Efficiency and Renewable Energy. The XPS experiments were carried out at the Environmental and Molecular Sciences Laboratory, a user facility of the Department of Energy, of the Pacific Northwest National Laboratory.

Appendix A. Supplementary material

Supplementary data associated with this article can be found, in the online version, at doi:10.1016/j.jcat.2011.11.015.

References

[1] R.R. Davda, J.W. Shabaker, G.W. Huber, R.D. Cortright, J.A. Dumesic, Appl. Catal. B 56 (2005) 171.
[2] J.W. Shabaker, G.W. Huber, R.R. Davda, R.D. Cortright, J.A. Dumesic, Catal. Lett. 88 (2003) 1.
[3] F.Z. Xie, X.W. Chu, H.R. Hu, M.H. Qiao, S.R. Yan, Y.L. Zhu, H.Y. He, K.N. Fan, H.X. Li, B.N. Zong, X.X. Zhang, J. Catal. 241 (2006) 211.
[4] A. Iriondo, V.L. Barrio, J.F. Cambra, P.L. Arias, M.B. Guemez, R.M. Navarro, M.C. Sanchez-Sanchez, J.L.G. Fierro, Top. Catal. 49 (2008) 46.
[5] P.N. Kechagiopoulos, S.S. Voutetakis, A.A. Lemonidou, I.A. Vasalos, Ind. Eng. Chem. Res. 48 (2009) 1400.
[6] X.H. Liu, K. Shen, Y.G. Wang, Y.Q. Wang, Y.L. Guo, Y. Guo, Z.L. Yong, G.Z. Lu, Catal. Commun. 9 (2008) 2316.
[7] K. Murata, I. Takahara, M. Inaba, React. Kinet. Catal. Lett. 93 (2008) 59.
[8] A. Tanksale, C.H. Zhou, J.N. Beltramini, G.Q. Lu, J. Incl. Phenom. Macrocycl. 65 (2009) 83.
[9] X.M. Wang, N. Li, L.D. Pfefferle, G.L. Haller, Catal. Today 146 (2009) 160.
[10] A. Iriondo, J.F. Cambra, V.L. Barrio, M.B. Guemez, P.L. Arias, M.C. Sanchez-Sanchez, R.M. Navarro, J.L.G. Fierro, Appl. Catal. B 106 (2011) 83.
[11] R.R. Davda, J.W. Shabaker, G.W. Huber, R.D. Cortright, J.A. Dumesic, Appl. Catal. B 43 (2003) 13.
[12] G.W. Huber, J.W. Shabaker, S.T. Evans, J.A. Dumesic, Appl. Catal. B 62 (2006) 226.
[13] E.L. Kunkes, D.A. Simonetti, J.A. Dumesic, W.D. Pyrz, L.E. Murillo, J.G.G. Chen, D.J. Buttrey, J. Catal. 260 (2008) 164.
[14] D.L. King, L. Zhang, G. Xia, A.M. Karim, D.H. Heldebrant, X. Wang, T. Peterson, Y. Wang, Appl. Catal. B (2010).
[15] Y. Sato, K. Terada, S. Hasegawa, T. Miyao, S. Naito, Appl. Catal. A 296 (2005) 80.
[16] W. Ruettinger, X.S. Liu, X.M. Xu, R.J. Farrauto, Top. Catal. 51 (2008) 60.
[17] D.A. Simonetti, E.L. Kunkes, J.A. Dumesic, J. Catal. 247 (2007) 298.
[18] K.G. Azzam, I.V. Babich, K. Seshan, L. Lefferts, Appl. Catal. B 80 (2008) 129.
[19] O.M. Daniel, A. DeLaRiva, E.L. Kunkes, A.K. Datye, J.A. Dumesic, R.J. Davis, ChemCatChem 2 (2010) 1107.
[20] T. Ebashi, Y. Ishida, Y. Nakagawa, S. Ito, T. Kubota, K. Tomishige, J. Phys. Chem. C 114 (2010) 6518.
[21] J.L. Xiao, R.J. Puddephatt, Coord. Chem. Rev. 143 (1995) 457.
[22] D.L. King, L. Zhang, A. Karim, Y. Wang, Prepr. – Am. Chem. Soc. Div. Pet. Chem. 56 (2011) 41.
[23] M. Chia, Y.J. Pagan-Torres, D. Hibbitts, Q.H. Tan, H.N. Pham, A.K. Datye, M. Neurock, R.J. Davis, J.A. Dumesic, J. Am. Chem. Soc. 133 (2011) 12675.
[24] C.S. Cao, G. Xia, J. Holladay, E. Jones, Y. Wang, Appl. Catal. A 262 (2004) 19.
[25] A.S. Arico, A.K. Shukla, H. Kim, S. Park, M. Min, V. Antonucci, Appl. Surf. Sci. 172 (2001) 33.
[26] W. Eberhardt, P. Fayet, D.M. Cox, Z. Fu, A. Kaldor, R. Sherwood, D. Sondericker, Phys. Rev. Lett. 64 (1990) 780.
[27] S. Hüfner, G.K. Wertheim, Phys. Rev. B 11 (1975) 678.
[28] A.S. Fung, M.R. McDevitt, P.A. Tooley, M.J. Kelley, D.C. Koningsberger, B.C. Gates, J. Catal. 140 (1993) 190.
[29] W.K. Shiflett, J.A. Dumesic, J. Catal. 77 (1982) 57.
[30] E.S. Shpiro, V.I. Avaev, G.V. Antoshin, M.A. Ryashentseva, K.M. Minachev, J. Catal. 55 (1978) 402.
[31] J. Fusy, M. Alnot, J. Jupille, P. Pareja, J.J. Ehrhardt, Appl. Surf. Sci. 17 (1984) 415.
[32] N.J. Luo, X.W. Fu, F.H. Cao, T.C. Xiao, P.P. Edwards, Fuel 87 (2008) 3483.
[33] G.D. Wen, Y.P. Xu, H.J. Ma, Z.S. Xu, Z.J. Tian, Int. J. Hydrogen Energy 33 (2008) 6657.
[34] A. Wawrzetz, B. Peng, A. Hrabar, A. Jentys, A.A. Lemonidou, J.A. Lercher, J. Catal. 269 (2010) 411.